ADVANCES IN MARINE CHEMISTRY
J. Blasco and J.M. Forja (eds.)

Scientia Marina 74S1
December 2010, 33-46, Barcelona (Spain)
ISSN: 0214-8358
doi: 10.3989/scimar.2010.74s1033

Carbonate system distribution south of the Canary Islands in spring 2000

IVÁN R. UCHA [1], MELCHOR GONZÁLEZ-DÁVILA [1],
MAGDALENA SANTANA-CASIANO [1], MARÍA JOSÉ RUEDA [2] and OCTAVIO LLINÁS [2]

[1] Departamento de Química, Universidad de Las Palmas de Gran Canaria, Campus de Tafira, Las Palmas 35017, Spain.
E-mail: mgonzalez@dqui.ulpgc.es
[2] Instituto Canario de Ciencias Marinas, Gobierno de Canarias, Las Palmas de Gran Canaria, Spain.

SUMMARY: The measurement of the surface molar fraction of CO_2 (atmosphere and sea water) and water column pH_T, total alkalinity, A_T, nutrients and oxygen were carried out in spring 2000 at the European Station for Time Series in the Ocean at the Canary Islands (ESTOC) and in the area located south of the Canary Islands. The significant eddy field strongly affecting the pattern of the chemical and carbonate system variables is presented and discussed. A mixing model based on the thermohaline properties of the water masses was established. The model explained over 97% of the variability found in the distribution of the chemical variables. Intermediate waters to the south of the Canary Islands show a high contribution of Antarctic waters with about 5% of pure Antarctic Intermediate Water. Moreover, the surface structure affected the atmosphere-ocean carbon dioxide exchange, making the area act as a CO_2 sink taking up 9.1 mmol m^{-2} $week^{-1}$, corresponding to 0.03 Mt of CO_2 which were taken up by the area in a week at the end of March 2000.

Keywords: carbonate chemistry, water masses, eddies, nutrients, oxygen, Canary Islands.

RESUMEN: Distribución del sistema del carbonato al sur de las Islas Canarias en la primavera del año 2000. – Durante la primavera del año 2000 se realizaron medidas en las aguas superficiales de la fracción molar de CO_2 (atmósfera y océano) y en la columna de agua de pH_T, alcalinidad total, A_T, nutrientes y oxígeno, para la Estación Europea Oceánica de Series Temporales de Canarias (ESTOC) y al sur de las islas Canarias. En este trabajo se presenta y discute el efecto del importante campo de remolinos presente en el área sobre la distribución de las variables químicas y del sistema de carbonato. Se ha establecido un modelo de mezcla, basado en las propiedades termohalinas de las diferentes masas de agua, que explica el 97% de la variabilidad encontrada en la distribución de las variables químicas. Las aguas intermedias al sur de las islas Canarias están caracterizadas por la alta contribución del agua Antártica intermedia diluida, que corresponde con una contribución próxima al 5% de agua Antártica intermedia pura. Por otro lado, las estructuras superficiales afectan al intercambio de CO_2 atmósfera-océano, actuando el área como un sumidero de dióxido de carbono incorporando 9.1 mmol m^{-2} $semana^{-1}$, que se corresponde con 0.03 MTon de CO_2 captadas por el área y en una semana a finales de marzo del 2000.

Palabras clave: química del carbonato, masas de agua, remolinos, nutrientes, oxígeno, Islas Canarias.

INTRODUCTION

The oceans have been divided into domains and provinces according to their ecological and physical features (Longhurst, 1998). The Canary Islands region is located in the westerly domain corresponding to the North Atlantic Subtropical Gyre province (NASE). This region is a transitional zone between the north-western African coastal upwelling region and the open ocean oligotrophic waters of the subtropical gyre. It is well known that the eastward flowing of the Azores Current splits into several southward branches (Reid, 1994). The branch which always flows eastward into the coastal upwelling region off northwest Africa is identified as the Canary Current. The islands present a barrier to this relatively weak equatorward flow of the Canary Current and to the flow of the trade winds due to the abrupt topography of the islands, which leads

to a variety of mesoscale phenomena south of the islands. These include a significant downstream wake (Arístegui *et al.*, 1994, 1997; Barton *et al.*, 1998; Davenport *et al.*, 1999) that has a great effect on the biogeochemical cycles of the region (González-Dávila *et al.*, 2003, 2006). Barton and Arístegui (2004) studied the changing properties of waters as they are advected towards the open ocean in filaments. They also investigated the exchange between filaments and eddies that re-circulated water parcels for several weeks.

Many researchers have studied the role of eddies that transport nutrients, taking the upwelled waters through the filaments to the oligotrophic area, including the Canary islands region (Falkowski *et al.*, 1991; McGillicuddy *et al.*, 2003; Arístegui *et al.*, 2004; Barton *et al.*, 2000; Barton and Arístegui, 2004) and the different upwelling cells (Cape Ghir, Cape Juby and Cape Bojador). Little work has been done on the effects of variability on the carbonate system. Most of the CO_2 work has been carried out in the northern part of the Canary Islands (Santana-Casiano *et al.*, 2001, 2007; Pérez *et al.*, 2001; González-Dávila *et al.*, 2003, 2007), where there is no island effect. Only González-Dávila *et al.* (2006) studied the effect of cyclonic and anticyclonic eddies on the nutrient pumping and on the upward displacement of dissolved inorganic carbon, observed from the northwest to the south central area of the Canary Islands. They also applied a model to determine the net inorganic carbon balance in a cyclonic eddy.

During the Poseidon 257 cruise, the area to the south of the Canary Islands was sampled in March 2000 as a hydrographic line crossing the multiple mesoscale features including cyclonic and anticyclonic gyres, filaments and wakes that affect the water mass transport and associated biogeochemical fluxes. The eastern North Atlantic area to the south of the Canary Islands (Fig. 1) is characterized by the presence of different water masses with thermohaline properties extensively described in the literature. In the upper waters two varieties of Eastern North Atlantic Central Water (ENACW), subtropical (tENACW) and subpolar (pENACW) (Harvey, 1982; Ríos *et al.*, 1992; Pollard *et al.*, 1996), have been defined at different isopycnal levels. The intermediate waters encountered to the south of the islands are influenced by the presence of diluted Antarctic Intermediate Water (AA) (Machín and Pelegrí, 2009) characterized by an oxygen-minimum and nutrient maximum domain, affecting intermediate water approximately to 20ºN (Speer, 1993, Reid 1994). The influence of Mediterranean water (MW) can be found in the Canary Islands from 900 down to 1800 m (Reid, 1994, Santana-Casiano *et al.*, 2001). The deep waters are dominated by the Northeast Atlantic Deep Water (NEADW) detected by the small variability and linearity in the thermohaline structure, which is divided into upper North Atlantic Deep Water (uNEADW) and lower Northeast Atlantic Deep Water (lNEADW) (Wright and Worthington, 1970).

The present study focused on the carbonate system to the south of the Canary Islands and the effect of the

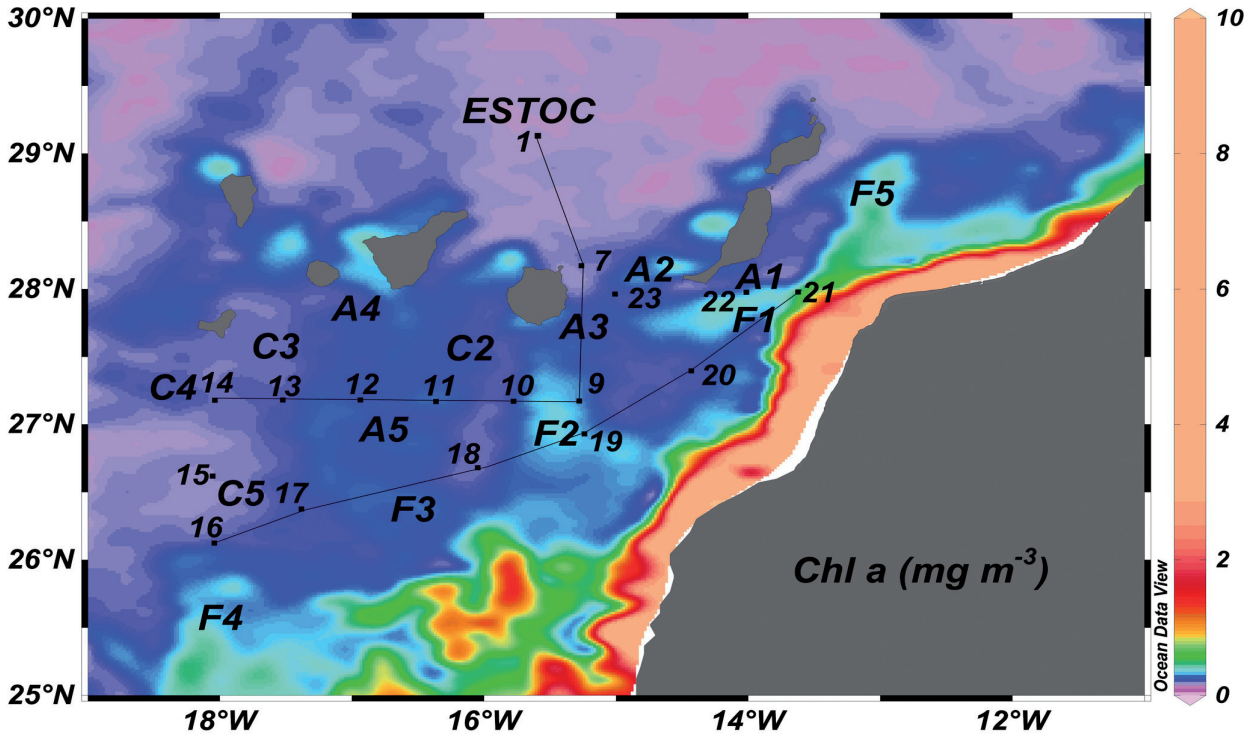

FIG. 1. – Satellite image from 19 March 2000 for the study area showing an important mesoscale structure south of the Canary Islands. Cyclonic (C) and anticyclone (A) eddy and filament (F) locations discussed in the text are labelled, as is the position of ESTOC site.

mesoscale structure on its variability. We used a mixing model based on the water masses present in the area, considering a set of vertically ordered mixing triangles to study the chemical variability of the water masses (Tomczak, 1981; Pérez *et al.*, 2001). A single and fixed temperature and salinity defined each water mass end-member in a triangle while a water mass showed a fixed TS relationship characterized by a mixing of two end-members. In order to improve our knowledge of the CO_2 system, the anthropogenic carbon fraction was studied using the TrOCA method (Touratier *et al.*, 2007). Special attention was paid to the spreading of AA in the area.

MATERIALS AND METHODS

pH

The pH in total scale (moles (kg sw)$^{-1}$) was measured following the spectrophotometric technique of Clayton and Byrne (1993) using the m-cresol purple indicator (DOE, 1994). The pH measurements were done with a system described in detail in González-Dávila *et al.* (2003). Repeated seawater measurements of different CRMs samples (n = 54) give a weighted standard deviation of ±0.002 pH units.

Total alkalinity

Total alkalinity of seawater (A_T) was determined by titration with HCl until the carbonic acid end point using two similar potentiometric systems, as indicated in Mintrop *et al.* (2000). The precision of the fit (s value) was better than 0.4 μmol kg^{-1} for the samples analyzed. The performance of the titration systems (±1.5 μmol kg^{-1}) was monitored by titrating different samples of certify reference material CRMs (#42) that have known C_T and A_T. Total alkalinity normalized to a constant salinity of 35 was computed where necessary ($NA_T = A_T / S \cdot 35$).

Total dissolved inorganic carbon

Total inorganic carbon (C_T) was computed from experimental values of pH_T and A_T, using the carbonic acid dissociation constants of Mehrbach *et al.* (1973) according to Dickson and Millero (1987). This set of constants showed the greatest agreement between C_T (pH, A_T) calculations and certified C_T values for CRM, batch 42, with a C_T residual of ±3 μmol kg^{-1} (n = 54). Total inorganic carbon normalized to a constant salinity of 35 was computed where necessary (NCT = CT /S · 35).

Partial pressure of CO_2 expressed as fugacity, fCO_2. CO_2 flux determination.

Fugacity of carbon dioxide (fCO_2) in air and in surface seawater is determined with a flowing system similar to the one designed by Wanninkhof and Thoning (1993), developed by Frank J. Millero's group at the University of Miami and described in detail in González-Dávila *et al.* (2003). The system was calibrated by measuring three different standard gases with mixing ratios of 0.0, 348.55 and 520.83 ppm CO_2 in air. Our system has a precision of less than 1 μatm and is accurate, relative to the standard gases, to 2 μatm. Fugacity of CO_2 in the seawater was calculated from the measured xCO_2 (mole fraction of CO_2 gas corrected to dry air and to the pressure of 1 atm).

The fluxes of CO_2 were calculated by

$$FCO_2 = K(fCO_{2,sw} - fCO_{2,atm}) \quad (1)$$

The CO_2 exchange coefficient K, in mol m^{-2} yr^{-1} μatm^{-1} was deduced as:

$$K = k \times S/11.1371 \quad (2)$$

where k in cm h^{-1} is the transfer velocity coefficient and S is the solubility in mol kg^{-1} atm^{-1} deduced from SST using polynomial coefficients after Wanninkhof (1992). 11.1371 is a conversion factor computed assuming seawater density of 1025 kg m^{-3}. k is deduced from satellite wind speeds at 10 m height, U_{10}, and SST using Wanninkhof (1992) k-U_{10} parameterization:

$$k_w = \left(0.31U_{10}^2\right) \times \sqrt{(660 / S_C)} \quad (3)$$

Wind speed was retrieved at a 25 km resolution from instantaneous 25 km scatterometer measurement, as indicated by Boutin and Echeto (1995), and was provided by LOCEAN, University Pierre et Marie Curie, http://www.locean-ipsl.upmc.fr. Gas solubility and Schmidt number, Sc, are computed for a constant salinity of 35 and for a sea surface temperature, SST, averaged over 1° and 1 month. The SST fields are the ones generated at the French National Meteorological Centre (NMC) by an optimal interpolation of AVHRR and in situ data (Reynolds and Smith, 1994).

Nutrients, chlorophyll *a* and oxygen

Samples for nutrients, chlorophyll *a* and oxygen were analyzed in the lab following the World Ocean Circulation Experiments (WOCE) standards (*WOCE*, 1994). For silicates, a modified Hansen and Grasshoff (1983) method was used, in which β-silicomolybdenic acid is reduced with ascorbic acid. The standard deviation for duplicates was 0.07 μmol L^{-1} for silicate, 0.06 μmol L^{-1} for nitrate and 0.01 μmol L^{-1} for phosphate. The standard error for five oxygen replicates was less than 2 μmol kg^{-1}. The chlorophyll *a* was measured using fluorometric analysis according to the methodology described by Welschmeyer (1994), using a TURNER™ 10-AU-000 fluorometer.

Mixing analysis

The contribution of the water masses $M_{k,i}$ considered for a given sample *i* can be calculated using the following linear equations:

$$\begin{aligned} 1 &= \sum M_{k,i} \\ S_i &= \sum M_{k,i} S_k \\ \theta &= \sum M_{k,i} \theta_k \end{aligned} \quad (4)$$

where *k* is the water mass and *i* is the sample number (from 1 to 368, in our study). S_k and θ_k are the thermohaline characteristics of the water mass end-member for each mixing triangle considered. Since the proportion of the water masses has to be calculated for all the samples, a non-negative least squares (NNLS) approach is used. The $M_{k,i}$ proportions for each sample were then applied to compute the expected concentration of any chemical variable for the water masses considered in the area by solving the 368 equations by the same NNLS method.

$$C_i = \sum M_{k,i} C_k \quad (5)$$

In order to know the sensibility of our final result of C_k with respect to the initial reference values of θ and S (after Perez *et al.*, 2001), we studied the error propagation through a Monte Carlo approach (Hammersley and Handscomb, 1964), considering the error in Table 1 in the initial reference variables θ and S obtained by applying an extended optimum multiparameter analysis (Álvarez *et al*., 2005) for the eastern North Atlantic. An extensive discussion of this methodology and its validity can be found elsewhere (Castro *et al.*, 1998; Pérez *et al.*, 1998; 2001); we followed the last recommendation by Pérez *et al.* (2001) and Álvarez *et al.* (2005).

RESULTS

Hydrography

A grid of 17 stations divided into 3 major lines was measured to the south of the Canary Islands (Fig. 1). Line 1 joined stations located at around 27ºN (sts. 9 to 14). Line 2 followed stations 16 to station 21 approaching the Africa coast, while line 3 crossed the area north to south from the ESTOC site (st. 1) to station 19 along 15ºW.

Upper thermocline distribution

SeaWIFS images (Fig. 1) revealed the spectacular scenario of a series of eddies spinning cyclonically (C) and anticyclonically (A) downstream of the islands of the Canary Archipelago. The strong upwelling cells located at Capes Juby and Bojador affected the area due to the generation of filaments reaching the field of eddies and interacting with them. Two filaments (F1 and F2) located near Cape Juby extended offshore and were traced to the southwest of Fuerteventura (F1), while F2 turned southward around the quasi-permanent cyclonic circulation (C1) trapped in the trough south of Gran Canaria. At their offshore limit, the anticyclone A3 was partly entrained around the anticyclone shed from the island of Gran Canaria. Another filament (F3) generated at Cape Bojador was observed to the south of Tenerife interacting with cyclonic eddy C5 and anticy-

TABLE 1. – Definition of source water types and their chemical properties (in μmol kg^{-1}) obtained from the mixing model using 359 water samples. Errors in *S* and θ after Álvarez *et al.* (2005).

	S	θ	O_2	AOU	NO_3	SiO_2
MMW	37.05±0.04	20.00±0.5	231±6	-3	0.2±0.1	0.3±0.05
tENACW	36.15±0.02	15.35±0.4	228±4	-1	7.2±0.9	1.8±0.30
H	35.66±0.02	12.2±0.4	190±2	71	13.3±0.9	5.0±0.60
pENACW	35.23±0.01	8.56±0.3	159±1	119	24.8±0.6	14.7±0.6
AA	34.9±0.02	6.5±0.1	116±2	184	29.3±0.2	20.3±0.3
MW	36.5±0.01	11.74±0.1	201±8	62	13.9±1.5	7.9±1.0
uNEADW	34.93±0.00	2.5±0.1	244±1	81	21.1±0.1	33.2±0.1
lNEADW	34.88±0.00	1.92±0.1	247±0	89	23.9±0.1	46.3±0.1
R^2			0.961		0.960	0.973
SD			8.36		1.37	1.72
	PO_4H_2	C_T	A_T	pH_T	$NC_{T,bio}$	$NC_{T,bio}$*
MMW	0.01±0.01	2082±12	2418±3	8.058±0.108	1979±2	1989[a]
tENACW	0.43±0.05	2130±7	2361±1	7.894±0.005	2007±4	2012±26
H	0.90±0.06	2150±6	2333±2	7.785±0.007	2049±3	2060±6
pENACW	1.51±0.04	2189±1	2325±2	7.674±0.004	2089±1	2087±3
AA	1.91±0.03	2221±1	2312±1	7.564±0.004	2092±1	2093±4
MW	0.71±0.08	2204±4	2414±3	7.827±0.012	2067±2	2067±7
uNEADW	1.39±0.00	2200±0	2341±1	7.723±0.001	2136±1	2133±3
lNEADW	1.59±0.00	2211±0	2360±0	7.722±0.001	2148±0	2149±1
R^2	0.963	0.961	0.972	0.983	0.973	
SD	0.10	7.62	3.82	0.012	6.82	

* Pérez *et al.*, 2001; [a] Álvarez *et al.*, 2005.

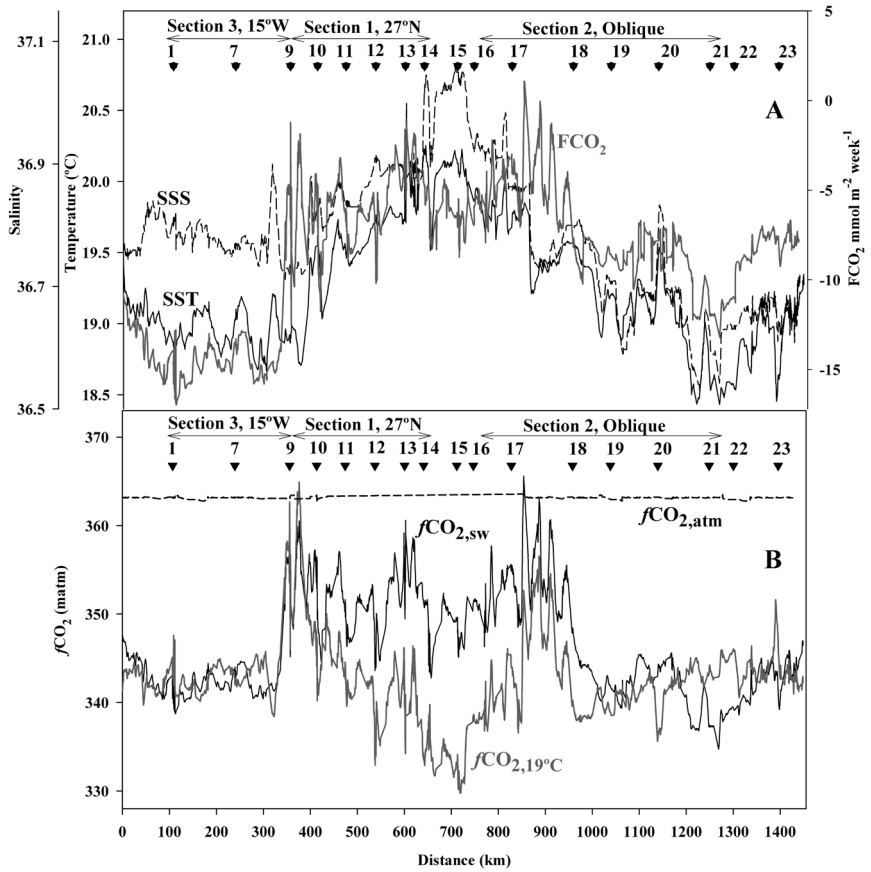

FIG. 2. – Distribution of A) sea surface temperature (SST), salinity (SSS) and CO_2 fluxes (FCO_2) using satellite wind speeds. B) CO_2 fugacity in the atmosphere ($fCO_{2,atm}$), in the ocean ($fCO_{2,sw}$) and normalized to 19ºC, ($fCO_{2,19ºC}$) along the cruise track. The main mesoscale structures are indicated together with the stations.

clone A5. A more complex structure was found south of 26ºN outside the area studied on this cruise. Line 1 ran westward along 27ºN between Gran Canaria and the outer island of El Hierro. It started close to the quasi-permanent feature observed south of Gran Canaria, anticyclone A3, but immediately went inside the coupled pair C2 and F2 and crossed between anticyclones A4 and A5. It moved into the area affected by cyclonic eddy C3 located east of El Hierro and finished close to cyclone C4, to the southwest of El Hierro. The oblique line close to the African coastline, line 2, started at the position of anticyclone A6 at 26°N, crossed cyclones C5 and C1 and intersected the filament generated at Cape Bojador F3 at around 17°W and those generated at Cape Jubi at 15.5°W and 15°W (F2 and F1) at the end of the line, where anticyclone A1 to the south of the Island of Fuerteventura is located.

Along line 1, the sea surface temperature (SST) (Fig. 2) increased from 18.7°C where filament F2 and cyclone C2 are located, close to station 10, to 20.25ºC before reaching station 14. At 17.5ºW, cyclone C4 injected warm surface seawater in the line located west of 18ºW, as can be seen in the SST images for the area (not shown), reaching a temperature of 20.25°C and a sea surface salinity (SSS) of 37.05. At 18ºW, the temperature and salinity fell dramatically by 0.75°C and 0.18, respectively, due to the presence of cyclonic eddy C4. Surface properties also showed the effects of filament F2 at 16°W and anticyclones A4-A5 at 16.5°W. The effect of the eddy field can also be clearly observed in the uplifted isosurfaces of temperature and density (Fig. 3), marking the strong cyclones C2 and C4, while the isolines deepened well below the mean for the line in anticyclonic eddy A4 and A5 at 17°W. In the shear area between C4 and A5 at 17.5°W, a deep chlorophyll maximum (DCM) was observed, with values of around 0.4 mg m^{-3} at 50 m depth, while the presence of F2 and C2 favoured a DCM above 0.50 mg m^{-3} at 50 m. The position of DCM in the water column was clearly related to the mesoscale structure, with the shallowest and largest DCM observed at the coldest temperatures at the limits of cyclonic eddies C2 and C4.

Starting at station 16, along Line 2 (Fig. 2) the temperature was 19.6°C and salinity was 36.9, lower values than those observed at station 15 (20°C and 37.04) at the west wall of our triangle, where A6 was located. These lower values at station 16 showed the effects of filaments originally formed within the Cape Bojador area. Temperature and salinity values showed an even greater reduction, associated with cyclonic

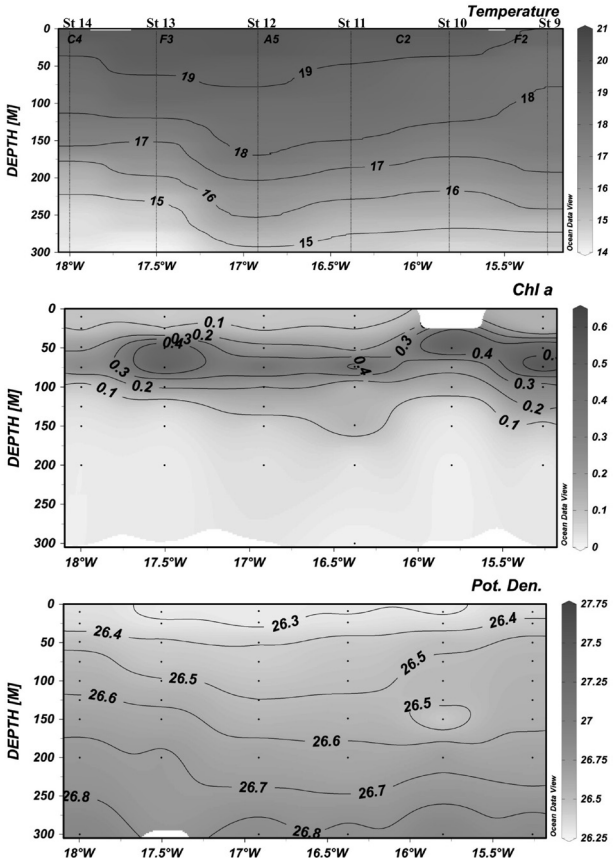

FIG. 3. – Temperature (ºC), chlorophyll *a* (mg m^{-3}) and potential density (kg m^{-3}) vertical profiles in the first 300 m (250 m for Chl *a*) along line 1 at 27ºN.

eddy C5 and the anticyclonic circulation of the F3–A5 filament-eddy system. After an increase in both SST and SSS related to the presence of A5, the line crossed filament F2 and cyclone C1, southeast of Gran Canaria, with a salinity of 36.59. At the end of the line, in the channel between Fuerteventura and Cape Juby, the effects of the presence of filament F1 were clearly observed in the presence of the coldest and freshest surface seawater in the area, with a SST of 18.45ºC and a salinity of 36.54. Low values were also observed to the west of station 21 up to 14°W, close to station 22, 60 miles off Cape Juby. Only at station 22, in the wake of Fuerteventura, did the temperature and salinity increase to 18.8ºC and 36.65. The effects of the structures observed along this line are also observed in the density anomaly graph (Fig. 4) when cyclones C5 and C1 cross. The sub-surface structure showed an overall deepening of the isopycnals to the southwest, indicative of the general offshore geostrophic flow. Little or no sign of chlorophyll fluorescence was evident near the surface in either filament. The DCM followed the base of the pycnocline, showing increased chlorophyll fluorescence at the border where the cyclones were located (Fig. 4), with values over 0.45 mg m^{-3} at 50 m where C1 met F2.

Line 3 along 15ºW (Fig. 2) had an SST of 18.8 (SSS of 36.77) at the ESTOC site (29.15ºN, 15.30ºW), decreasing south of 28ºN due to the effect of F1 trapped between C1 and A2. After briefly crossing the warm and salty area generated by anticyclone A3, the line showed a lower SST and SSS again due to the effect of F2 at 27ºN.

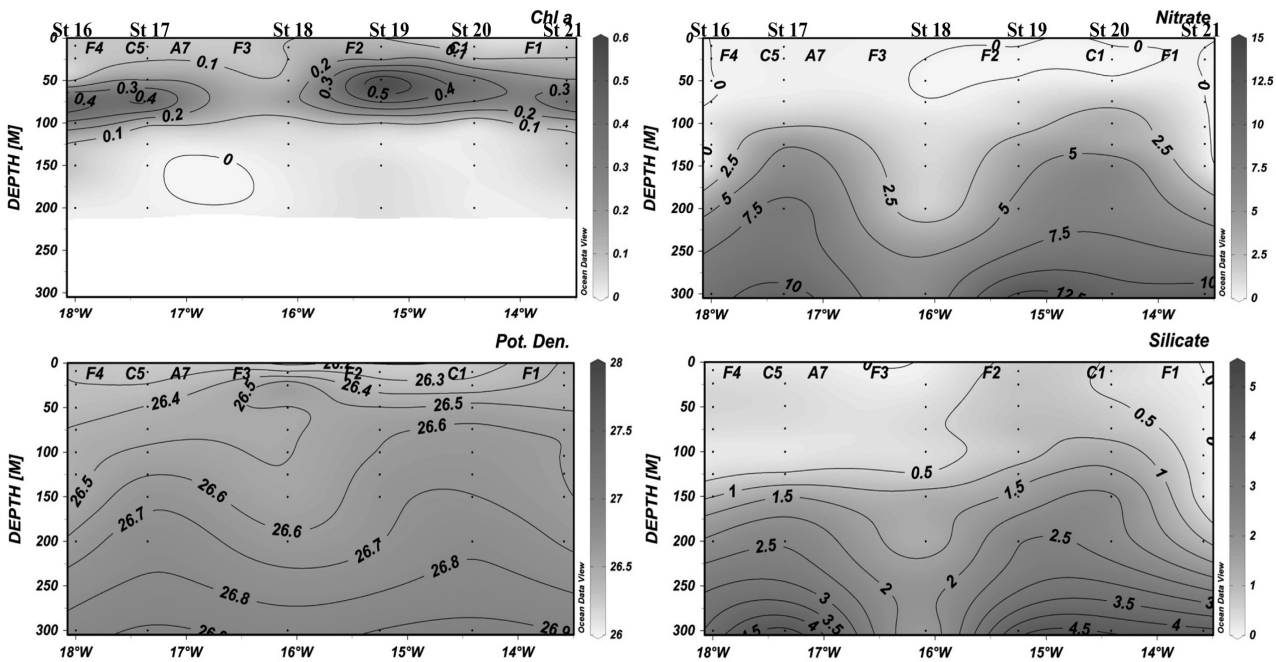

FIG. 4. – Chlorophyll *a* (mg m^{-3}), potential density (kg m^{-3}), nitrate+nitrite (μmol kg^{-1}) and silicate (μmol kg^{-1}) in the upper 300 m along the oblique line 2, as indicated in Fig. 1

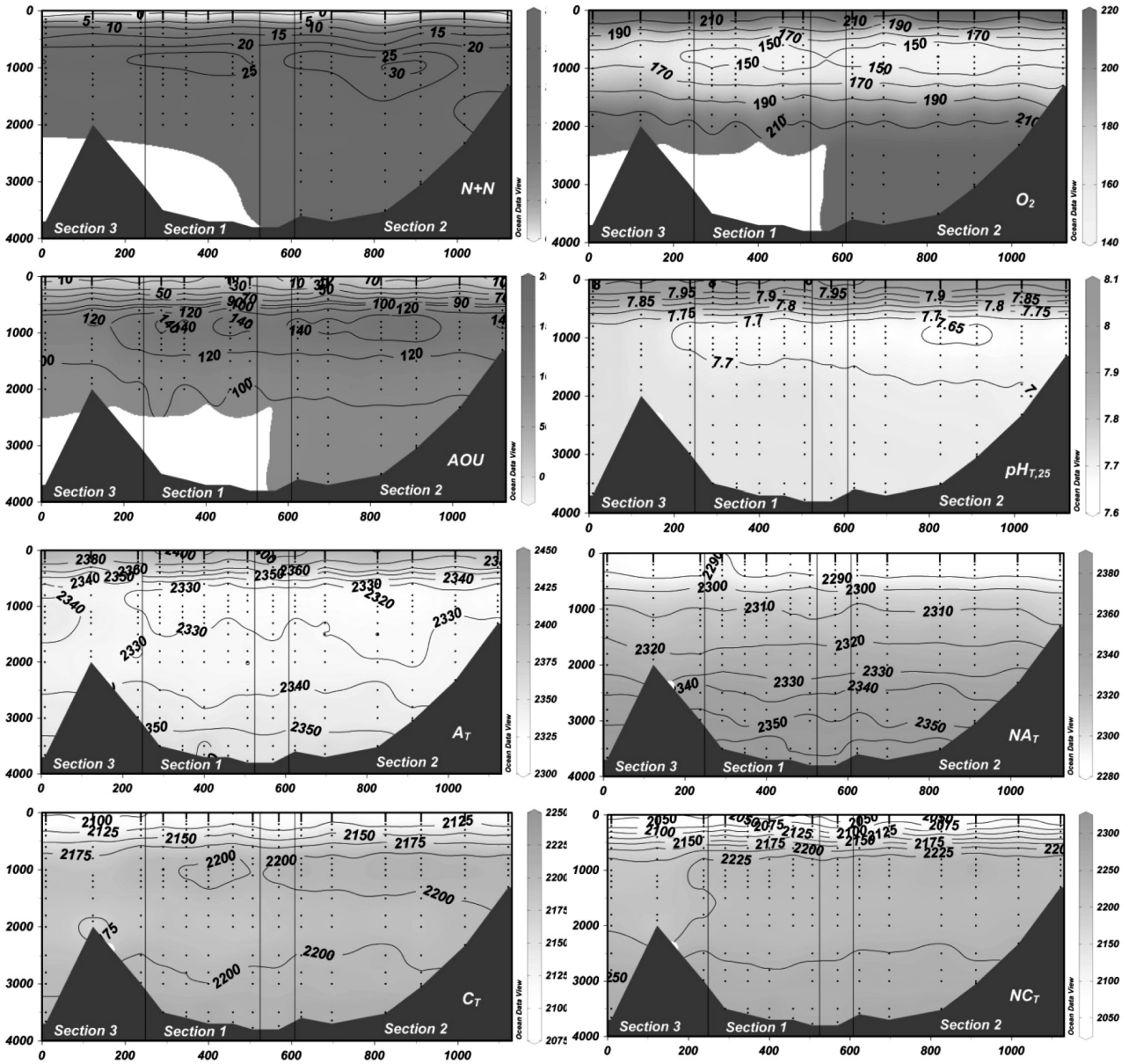

FIG. 5. – Nitrate and nitrite (N+N), oxygen (O_2), apparent oxygen utilization (AOU) and carbonate variables, pH in total scale at 25ºC, total alkalinity (A_T), total dissolved inorganic carbon (C_T) and normalized to a constant salinity of 35 NA_T and NC_T from ESTOC station to station 21 following the cruise track. The three lines indicated in Figure 1 are labelled.

The presence of these mesoscale structures also affected the pattern of vertical distributions of nutrients, oxygen and carbonate system parameters in the area (Fig. 4 and 5). Nitrate plus nitrite (N+N), phosphate (not shown) and silicate were nearly zero at surface but were affected by the presence of cyclonic eddies and filaments and then increased with density along the water column (with a maximum around 1000 m). Values of N+N at 150 m depth for the ESTOC station, north of the Canary Islands and outside the field of eddies, were close to 1.25 μmol kg^{-1}. However, at the stations located on the cyclonic eddies C1 (st. 20), C5 (st. 17) and C4 (st. 14) values at 150 m reached, respectively 4.18, 5.85 and 4.40 μmol kg^{-1}, contributing to higher chlorophyll levels in this area. These values were found at around 200 m for the ESTOC station. The position of the DCM is located at 70 m, in the strong boundary and shearing area between cyclone C4 and anticyclone A5 (st. 13 and st 14, Fig. 3). However, the presence of the moderate thermocline hinders the manifestation of eddies in the upper 50 m, limiting the effects on the distribution profiles. Phosphate distribution (not shown) is very similar to nitrate distribution, with a high correlation between them (r^2 = 0.99, N:P = 16.3 ± 0.1, N = 335). In order to study the effect of nutrient input on phytoplankton growth inside the eddy

field, it is important to determine the ageing status of a given upwelled water mass parcel. Whereas young upwelled water contains nutrients mostly in dissolved inorganic forms, aged upwelled water has had its nutrients transformed into organic forms. We applied the ageing upwelling index (AUI_C) of Takahashi *et al.* (1993) following the nomenclature of degree of nutrient consumption (DNC_C) of Chen *et al.* (2004)

$$DNC_C = AUI_C = 0.7 \text{ Chl } a / ((N+N) + 0.7 \text{ Chl } a) \quad (6)$$

where the constant 0.7 is a conversion factor between chlorophyll *a* (in mg m^{-3}) and inorganic nitrogen (in μmol l^{-1}) and is assumed to be similar to that reported in the above two studies. DNC_C is nearly zero in newly upwelled water due to the fact that there is an insignificant amount of phytoplankton. If there are large amounts of chlorophyll and low nutrients due to active phytoplankton uptake, DNC_C is 1 in the old upwelled water. DNC_C was relatively low in the area of eddies (data not shown) with values below 0.45 at stations 10, 17 and 19. Only stations 13 and 14 at the position of C4 showed DNC_C values of 0.85 at 75 m, indicating older upwelled water associated with this gyre.

Deep water distribution

Along the water column (Fig. 5), maximum values and variability are observed as a result of the presence of nutrient-rich AA and nutrient-poor MW. NADW is characterized by a relatively constant N+N value of around 20 μmol kg^{-1}, a phosphate value of 1.4 μmol kg^{-1} and silicate concentrations increasing rapidly to a maximum value of 25 μmol kg^{-1} at 2000 m (data not shown). The maximum nutrient values at around 1000 m were not so evident at ESTOC and station 7, indicating very low if any AA contribution.

Figure 5 shows the distribution of the carbonate system variables, A_T, pH_T and C_T, over the selected lines. Using data from the surface to 400 m, total alkalinity was clearly related to salinity in this area: A_T = 146 (±19) + 61.31 (±0.52) · S (r^2 = 0.989, N=162) STD = 2.39 μmol kg^{-1}. After normalization to a constant salinity of 35, NA_T showed a constant value of 2286 ± 3 μmol kg^{-1} down through the first 200 m. A steeper vertical gradient of NA_T in all lines was observed below the main thermocline. The correlation between NA_T and silicate distribution was as high as r^2 = 0.95 with n = 362 and an NA_T/SiO_2 ratio of 1.77 ± 0.03, a slope that also depends on the mixing of water masses with contrasting preformed levels of alkalinity and silica. The similar rate of dissolution of hard biogenic structures—both calcium carbonate and opal affect the alkalinity and silicate distribution, respectively—may account for the observed relationship. The ENACW showed a gradient in NC_T, nutrient and apparent oxygen utilization (AOU), with values increasing from the surface down to 800 m. A maximum was observed in all the nutrients at 900-1000 m related to the presence of AA characterized by a minimum in salinity (35.142 at st. 12) and in oxygen, reaching values of 120 μmol kg^{-1} and an AOU of 160 μmol kg^{-1}. pH_T at 25°C showed an inverse correlation with AOU, indicating the presence of AA south of the Canary Islands at around 900 m, with values as low as 7.62 at stations 18 and 19 and below 7.66 for all the stations in that region. The pH_T value at the ESTOC site at 900 m was 7.73. At deeper levels, the MW signal is discerned by its moderate AOU values, higher pH_T values and lower nutrient concentration and NA_T and NC_T values. Below these intermediate waters a relatively homogeneous layer of nutrients, pH_T and AOU reaching 2000 m is observed. Below 2000 m, NADW is characterized by high nutrients and a low AOU of 100 μmol kg^{-1} and a pH_T of 7.72, slightly higher at the stations to the north of the Canary Islands. The increase in NC_T with depth of 40 μmol kg^{-1} below 2000 m is related to the carbonate dissolution.

Fugacity and fluxes of CO_2 in the area

Figure 2 presents fCO_2 surface seawater and atmospheric values between 14 and 22 March 2000 at 5 m depth together with SST and SSS. The effect of the mesoscale structure in the area made the surface fCO_2 reach higher values for cyclonic eddies. These higher values were, however, associated with lower temperature values related to uplifted seawater. Vertical mixing should bring subsurface CO_2-rich waters upwards, since C_T and fCO_2 increases vertically with depth (Fig. 5). This carbon dioxide will be reduced by biological activity. In an oligothrophic area such as the Canary Islands only a fraction of this inorganic carbon will be used. Moreover, vertical mixing could bring inorganic carbon into the mixing layer in greater proportions than those established by Redfield, leaving residual carbon that cannot be eliminated by new production.

Seawater fCO_2 values along the cruise line were below the atmospheric fCO_2 value of 363 ± 1.2 μatm. Only between stations 17 and 18, affected by both cyclone C5 and filament F3, were values in seawater similar to those in the atmosphere. Moreover, the area along line 1 and 2 was the most strongly affected by the mesoscale structure for the area. Initially, line 3 along 15°W from the ESTOC station to station 9 showed relatively stable values, with $\Delta fCO_2 = fCO_{2,SW} - fCO_{2,atm}$ of -17 μatm. Only when the ship crossed warm and saltier waters injected by the action of A3, and went inside the effects of filament F2 around station 9, did the $fCO_{2,SW}$ increase by 15 μatm. Along line 1, the SST increased by about 1°C from east to west but was affected by the mesoscale structure, with a strong correlation between SST and fCO_2. Along line 2, the highest heterogeneity was observed between stations 17 and 18, where the effects of filaments of the original cell F3 with lower temperature were not correlated with lower fCO_2 values. After station 18 and up to station 23, the high variability observed in the SST and SSS values was

not correlated with fCO_2 values, showing a relatively constant value of 342 ± 2 μatm. In order to thoroughly understand this effect, fCO_2 values were normalized to the average temperature for the area during this period, 19°C, as is also depicted in Figure 2. Considering a relatively constant contribution of the fCO_2 variability by CO_2 atmospheric-oceanic exchange in this area, the observed behaviour must be due to the counterbalance between increased fCO_2 waters coming from vertical mixing inside a gyre and from filaments of upwelled waters, and decreased fCO_2 waters after primary production favoured by increased nutrient injection by the same two processes. Part of the fCO_2 variability in the area was removed after considering solubility effects through temperature correction. Only the area between stations 9 and 10 and the area between stations 17 and 18 kept high fCO_2 values. The effect of filament F2 trapped by C1 and C2 (Fig. 1) introduced in the area between stations 9 and 10 upwelled waters with higher carbon content that was not removed by primary productivity. The values were 20 μatm higher than those outside the cyclone area. If we apply the linear relationship observed between A_T and salinity (see above) for the continuous SSS values together with surface fCO_2, the computed C_T (data not shown) at stations 9 and 10 increased by over 10 μmol kg^{-1}, from 2093 μmol kg^{-1} for the surrounding area to 2104 μmol kg^{-1} at station 9. Moreover, the $pH_{T,25}$ was reduced in 0.02 units clearly indicating the arriving of subsurface CO_2 rich waters. The same behaviour was observed for filament F3 when stations 17 and 18 were crossed, with fCO_2 values 15 μatm higher, total inorganic carbon 8 μmol kg^{-1} higher and 0.02 pH units lower than surrounding waters. It can be observed that the area affected by upwelling and filaments generated along the African coast between Cape Juby and Cape Bojador at the end of March (sts. 16-22) showed slightly lower fCO_2 values and the lowest inorganic carbon concentration (around 2087 μmol kg^{-1}) in the area (data not shown), indicating higher inorganic carbon utilization. However, the inorganic carbon introduced in the surface waters due to upwelling was not being removed at all, at least at this time of the year, by the enhanced primary productivity due to the injection of nutrients to the euphotic layer.

The values of ΔfCO_2 between the seawater and the atmosphere were used to estimate CO_2 fluxes in the area for the study period (Fig. 2), following the calculation indicated in the experimental section. The whole area acted as a sink of CO_2 taking up 9.1 mmol m^{-2} $week^{-1}$ during the week in which the cruise was carried out. The average wind speed for the week of 14 to 22 March 2000 ranged only from 10 to 15 km h^{-1}, a calm period that produced low CO_2 fluxes. Values reached -15 mmol m^{-2} $week^{-1}$ north of the Canary Islands, related to higher wind speeds, while the values were -10 mmol m^{-2} $week^{-1}$ after station 18, with similar ΔfCO_2 as in the north line but with lower wind speeds. Fluxes of about -5 mmol CO_2 m^{-2} were determined along line 1

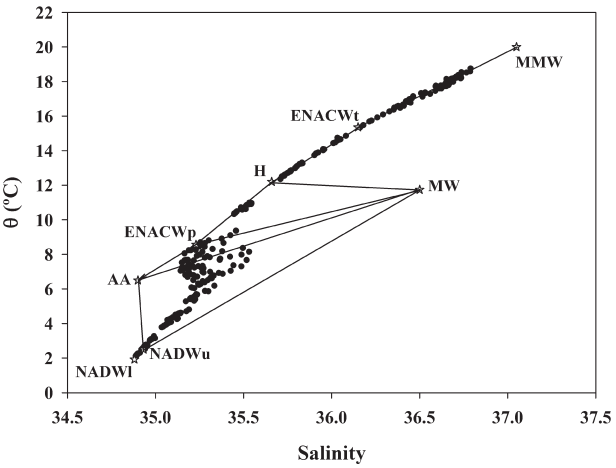

FIG. 6. – θ-S diagram using the bottle data, the thermohaline properties of the different water types indicated as starts and the applied mixing triangles used in the mixing model. Madeira Mode Water (MMW), subpolar East North Atlantic Central Waters (pENACW) and subtropical East North Atlantic Central Waters (tENACW), H end-member, Mediterranean waters (MM), Diluted Antarctic Water (AA) and North Atlantic Deep Water divided into upper and lower limits, uNADW and lNADW, were considered. ESTOC data were resolved by replacing the AA point with pENACW.

and were directly controlled by the atmosphere-ocean CO_2 gradient. Only close to station 17, where filament F3 affected the surface distribution, was a zero flux determined. Assuming that the values presented in this study are representative of the area to the south of the Canary Islands of 2° latitude and 4° longitude, a total of 0.03 Mt of CO_2 were taken up during that week. The value was not extrapolated to a per year data due to the strong seasonal cycle observed for the carbonate system variables in the ocean (González-Dávila *et al.*, 2003; Santana-Casiano *et al.*, 2007).

DISCUSSION

Figure 6 shows a potential temperature(θ)-salinity diagram for bottle samples collected during the cruise together with the characteristics of the source water types (Table 1). The ENACW were divided into two segments, subpolar (pENACW) and subtropical (tENACW) mode waters. The study area is affected by the formation of Madeira Mode Water (MMW) (Siedler *et al.*, 1987). Consequently, we considered the θ-S properties for the tropical ENACW segment as 15.35°C and 36.15, (Álvarez *et al.*, 2005). Following Harvey (1982), we chose 12.2°C and 35.66 as H end-member to separate tENACW and pENACW. The pENACW properties were described by Castro *et al.* (1998), with a potential temperature and salinity of 8.56°C and 35.23, respectively (Table 1). We also used θ and salinity values of $NADW_u$ and $NADW_l$ suggested by Castro *et al.* (1998) for the upper and lower limits. The termohaline characteristics of MW were selected from Wüst and Defant (1936) (Table 1).

Only station 1 (ESTOC) showed a minimum of salinity and pH_T at 800 m (Fig. 5 and 6) of 35.4 and

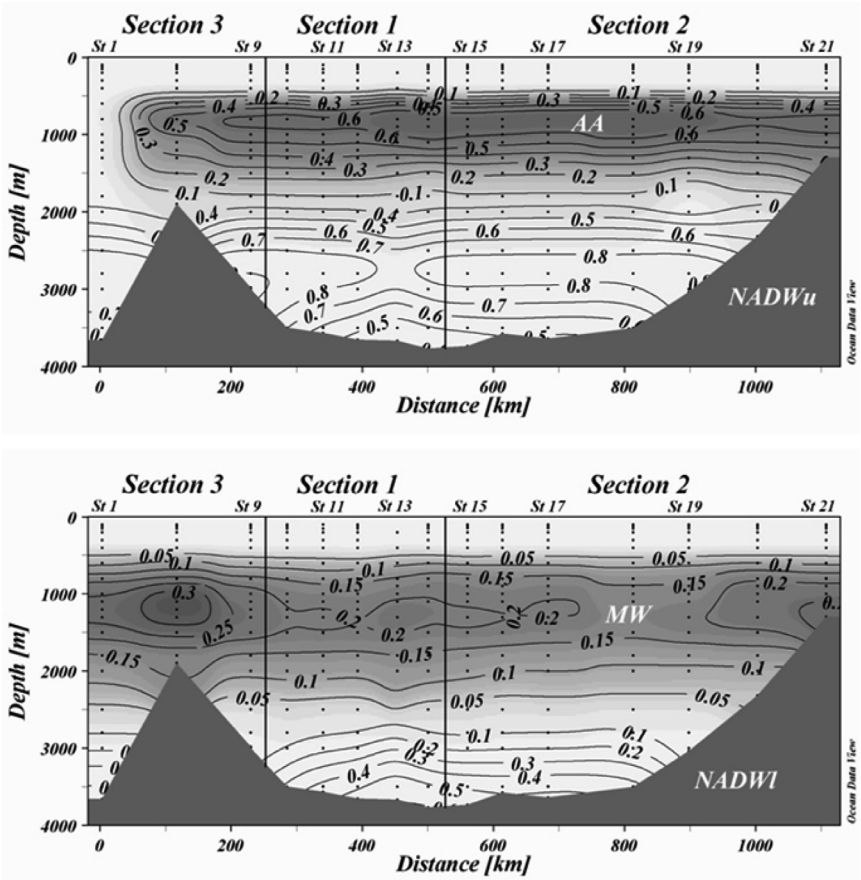

FIG. 7. – Water mass contribution from the ESTOC station to station 21 following the cruise track. Upper panel: Diluted Antarctic Water (AA) and upper North Atlantic Deep Water (uNADW). Lower panel: Mediterranean Water (MW) and lower North Atlantic Deep Water (lNADW).

7.72, respectively, indicating the absence of any influence of AA. At this site, the existence of $NACW_t$, H, pENACW, MW, $NADW_u$ and $NADW_l$ water masses is well known (Pérez *et al.*, 2001; Alvárez *et al.*, 2005). To the south of the Canary Islands, as stated above, the influence of AAIW was considered. In this study we refer to the *diluted*-AA (about 11% of pure AAIW) encountered in the North Atlantic at 20°N with the θ-S characteristics of 6.5°C and 34.9, in agreement with earlier studies in the area (Fraga *et al.*, 1985; Tsuchiya *et al.*, 1992; Pérez *et al.*, 2001, Alvarez *et al.*, 2005). The contributions of ENACW and NADW waters were computed by the straight equation line from H-tENACW and NADWu-NADWl, respectively. The samples from sea surface to the first 100 m were excluded from the analysis because their thermohaline properties had been altered by atmospheric conditions.

A sensitivity study of our approach was done for an estimation of error propagation in the chemical variable through the proportion of computed $M_{k,i}$ (presented in Table 1), as indicated in the experimental section. The error in the input variables is smooth transmitted to our chemical parameter determination and presented in Table 1. Moreover, a sensitivity study was also carried out for the presence or absence of water masses and for the structure of the mixing triangles. A particular study was made for the presence of Labrador Sea Water (LSW). Several authors (Käse *et al.*, 1986; McCartney and Talley, 1992, Alvarez *et al.*, 2005) have reported the influence of LSW close to the islands. The LSW reaches the African coast after a long excursion along a cyclonic gyre and mixing with MW (Paillet *et al.*, 1998). In the area considered in this study south of the Canary Islands, the results indicated (data not shown) that the inclusion of this water mass does not improve the mixing model output, and it was therefore not considered.

The estimated error for each chemical variable is within the experimental error and accurately supported the reference θ and S values used in our calculation. Nitrate, oxygen and C_T in subsurface waters vary due to the remineralization of organic matter (ROM) and calcium carbonate dissolution. Therefore, they do not completely behave as conservative variables. Thus, we should expect a lower percentage of explained variance for these chemical properties due to these two processes.

In order to determine preformed values for the total inorganic carbon, the *AOU* was used to correct the C_T values for the remineralization of the organic matter

$$C_{Tbio} = C_T - (AOU/R_C) \quad (7)$$

where the stoichiometric coefficient R_C corresponds to the revisited Redfield ratios estimated by Fraga *et al.* (1998). The excess carbon in the water column coming from anthropogenic input was computed using the improved TrOCA approach (Touratier *et al.*, 2007), where four known properties are needed (θ, C_T, A_T and O_2).

The distribution of water mass contribution along the stations sampled from the ESTOC site to station 21 using the θ and S pairs of data is presented in Table 1 and plotted in Figure 7. The mode of tENACW (not shown) predominated between 200 and 500 m, while the polar mode water was found below the subtropical water at the ESTOC site. The salinity maximum etween 700 and 1500 m was associated with MW centred at about 1250 m, with a contribution of up to 30% at the ESTOC station and between Gran Canaria and Fuerteventura, and below 20% in the southern part. Situated at around the same depth, the AA occupied the region to the south of the Canary Islands from east to west. The AA characteristics used in our study were those observed at 20ºN, where this water dilutes rapidly with ENACW (Reid, 1994), contributing in this area with values of around 70%, characterized by high nutrient, high apparent oxygen utilization and low pH at the salinity minimum. The highest values of AA contribution were found at 17.5°W in line 1 at 27°N, while relatively constant values of around 70% were observed along the oblique line, with the highest values at the stations closest to the African slope. The northward spreading of AAIW was claimed to reach 28.5°N by Pérez *et al.*, (2001), while Álvarez *et al.* (2005) placed the limit at the Azores current at 35ºN. Our results showed evidence that the AA flows northward of the Canary Islands along the African coast with a significant signal (Machín and Pelegrí, 2009 and references therein), characterized by a minimum in salinity and a maximum in silicate but, more importantly, by a minimum in pH_T values of 7.62-7.65 μmol kg^{-1}. North of 28ºN the mixing among AA with ENACW and MW affected the seawater properties and did not allow us to obtain any signal at the ESTOC site at this time (Santana-Casiano *et al.*, 2007). Only along the African coast were values as high as 70% for the AA contribution observed at 28ºN at the northernmost station (St. 21). The uNEADW is centred at 2800 m over the whole area, with a contribution of 80%, while the lNEADW is present below 3000 m, reaching over 40% at the bottom.

Table 1 presents the nutrient, oxygen and carbonate system end-members which were determined after applying the mixing model. The variances explained by the model are greater than 96%, even considering the low number of samples used to determine the properties of pENACW and NADW. The ratios of variance not explained by the model are $\Delta P:\Delta N:\Delta C:\Delta O_2 \equiv 1:15:81:90$ (Table 1), being of the same order as the stoichiometric ratios. A_T end-members, and particularly pH_T end-members and residuals, are close to the analytical errors and the model defined its natural variability. Nutrient and pH_T end-members summarized the chemical variability of the water masses. At the upper limit of the subpolar waters, in this area H showed relatively high values for all the chemical characteristics, and in particular AOU, in comparison with other studies for the Canary region (Pérez *et al.*, 2001, Álvarez *et al.*, 2005). The AA end-member showed the highest AOU values in the intermediate and deep water region because it is the oldest and in its trajectory crosses areas with strong biological activity. The same explanation is applicable to its low pH and high C_T and nutrient concentration.

The mixing model removed the variability caused by mixing. The residual variability can be mainly attributed to either ROM or dissolution of hard parts of biogenic matter. Oxygen, pH_T, nitrate and C_T are the variables most affected by ROM while redissolution increases silicate, C_T and A_T. The correlation between phosphate and nitrate residuals (data not shown) is $r^2 = 0.38$, with an N:P ratio of 14.7 ± 0.6. The AOU and nitrate also showed a significant correlation ($r^2 = 0.42$), with an R_N of 6.2 ± 0.5, which is lower than was expected from ROM. The AOU and C_T residuals showed an R_C of 1.1 ± 0.06, with a correlation of $r^2 = 0.48$, which is also lower than that expected from ROM (Ríos *et al.*, 1998). The high productivity of the upwelling area along line 3, close to the African coast, and the regions located around the permanent features to the south of the Canary Islands contributed to the increase in nutrients in these areas. Furthermore, the diluted AAIW located to the south of the Canary Islands (Fig. 7) also showed a maximum ROM with negative anomalies for pH_T (over 0.015) and positive C_T (over 9 μmol kg^{-1}), AOU (reaching 14 μmol kg^{-1}) and less important results for nitrate (around 1 μmol kg^{-1}) centred at around 900 m depth (data not presented). The bottom layer was characterized by relatively low ROM.

In order to remove re-mineralization and re-dissolution effects on C_T end-members, Table 1 also presents the corresponding $C_{T,bio}$ (Eq. 7) end-members. After normalization to a constant salinity of 35, our values for $C_{T,bio}$ end-members showed a good correlation with θ ($r^2 = 0.962$) and agreed with values obtained by other authors in the eastern Atlantic (Table 1). Our value for the AA of 2092 μmol kg^{-1} is in excellent agreement with values for other cruises to the south of the Canary Islands region (Table 2 in Pérez *et al.*, 2001). AAIW in its formation area at the sub-Antarctic Front (SAF) showed values of $C_{T,bio}$ = 2165 μmol kg^{-1} (Le Groupe CITHER-3, 1998). During its transport, it is mixed with South Atlantic Central Waters and NADWu, which dilute its properties from 100% at the SAF to 45% at 24ºN (Pérez *et al.*, 2001) when linear mixing was assumed between AAIW and pENACW at 40ºN (9.4ºC, salinity 35.3 and $C_{T,bio}$ = 2085 μmol kg^{-1}). Our mixing model indicated that at the depth of the salinity and pH minimum this diluted AA contributed 70% to the seawater observed to the south of the Canary Islands. That means that the average percentage of pure AAIW

in the area was only around 5% compared with 45ºN at 24ºN and the high nutrient and inorganic carbon values for the AA in our area are the result of remineralization along its long northward trajectory and enrichment due to southward transport of high nutrient, AOU and C_T upwelled waters off northwest Africa.

Mediterranean waters showed similar $C_{T,bio}$ values (Table 1) to the 2067 μmol kg^{-1} reported by Pérez *et al.* (2001) and the 2062 μmol kg^{-1} reported by Álvarez *et al.* (2005), with waters slightly more ventilated during our cruise, as suggested by the oxygen content (201 vs 192). Part of this difference could be compensated by anthropogenic CO_2 input and also by the presence of eddies in the area that can inject younger MW in the basin. Both NADW end-members were well related to other values in the literature (Table 1, see also Table 2 in Pérez *et al*., 2001). Our data for NADWl showed higher (by 5%) silicate values than data obtained from the north of the Canary Islands. This may be the result of a deep silica maximum along 24ºN that increased the values compared with those to the north of the Archipelago, as described by Reid (1994). A similar mixing analysis has been made in other areas of the Eastern North Atlantic Basin by several authors, most of them being summarized in Pérez *et al.* (2001) and Álvarez *et al.* (2005). The end-members showed very good agreement for the different data bases. However, the values for tENACW are not comparable because Madeira Mode Water was included in our study and not considered together with tENACW. The AA end-member observed during this cruise gave higher differences than cruises to the north of the Canary Islands, where the influence of AAIW is smaller.

Anthropogenic carbon (C_{ANT}) penetrated deeper than the depth corresponding to the main thermocline in the Canary Island area, as shown in Figure 8. C_{ANT} is expected to accumulate within the subtropical gyres, where Ekman convergence is important. The youngest waters (i.e. those which recently lost contact with the atmosphere) are heavily contaminated by C_{ANT}. The formation of NADW within Greenland and Norwegian seas and its transport by the Deep Western Boundary Current (DWBC) are responsible for the deep and intense penetration of anthropogenic carbon in large parts of the northern hemisphere. Upper C_{ANT} estimations were disregarded due to oxygen oversaturation, as they would lead to an overestimation of C_{ANT}. The values at 100 m (average mixed layer depth) were extrapolated to the surface. The waters belonging to NACW are characterized by a

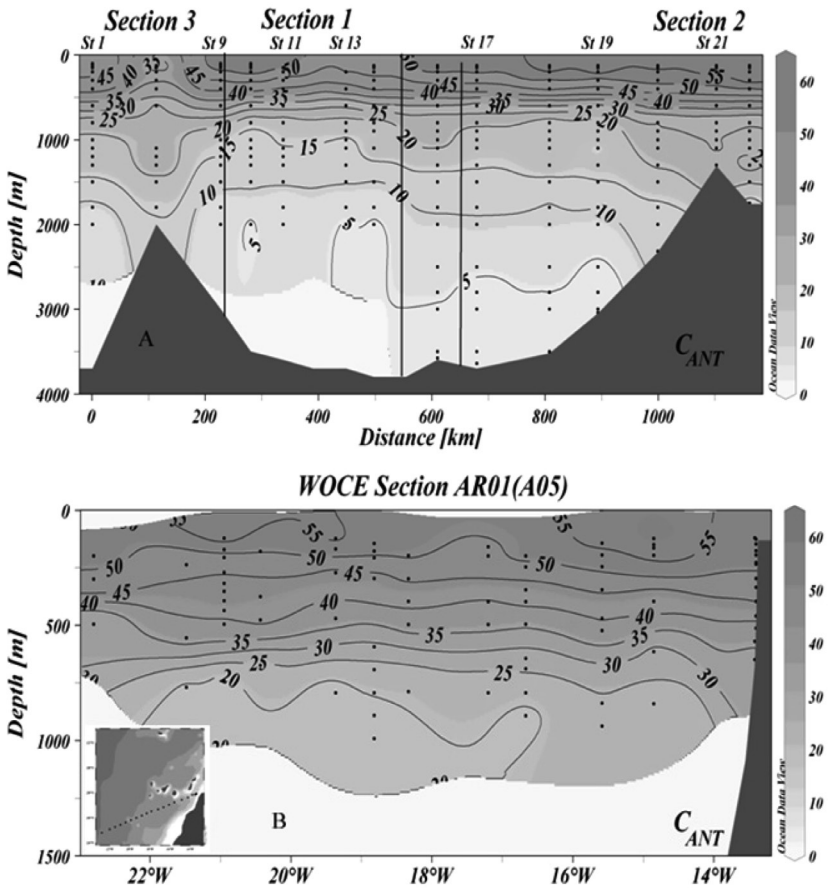

FIG. 8. – Distribution of the C_{ANT} (μmol kg^{-1}) using the TrOCA approach: A) the whole area, from the ESTOC station to station 21 following the cruise track, B) the WOCE Line AR01 (A05) in 1998. Data from http://cdiac.ornl.gov/oceans/woce_a25.html

high concentration of C_{ANT}, with values of around 60 μmol kg^{-1} at the base of the mixed layer and reaching 40 μmol kg^{-1} at 500 m. At a depth of around 900 m, the influence of the oldest AAIW can be observed by low C_{ANT} values of 10 μmol kg^{-1}, reaching uncontaminated waters below 1500 m. Water located at the ESTOC site with a higher MW influence showed a higher C_{ANT} penetration due to its higher content when it is formed in the Gulf of Cadiz.

Line 3 of POS257 was compared with WOCE Line AR01 (A05) (http://cdiac.ornl.gov/oceans/woce_a25.html), carried out in January 1998 (Lee *et al.,* 1998) and focusing on following the interannual variability of C_{ANT}. The results show (Fig. 8b) the consistence between the two cruises, with values within the uncertainty in the back calculation technique of anthropogenic carbon through the TrOCA method (±6.25 μmol kg^{-1}) (Touratier *et al.*, 2007), although an increase in C_{ANT} over the years is expected.

CONCLUSIONS

The biogeochemical distribution to the south of the Canary Islands is strongly influenced by the series of eddies spinning cyclonically and anticyclonically downstream of the islands of the Canary archipelago together with filaments generated in the upwelling cells located at Capes Juby and Bojador, which interact with the eddy field. The aging index of upwelling indicated relatively new upwelled waters in the area. Only stations located to the westernmost points showed the oldest upwelled waters. The pH_T at 25ºC appeared as an important water mass indicator for AA with values as low as 7.62 and always below 7.66 for the stations to the south of the Canary Islands. The pH_T at the ESTOC site at 900 m was 7.73.

The application of a simple mixing model for the water masses found to the south of the Canary Islands in March 2000 explained more than 96% of the chemical variability. The AA end-member showed the highest AOU values in the intermediate and deep water region because it is the oldest and in its trajectory it crosses areas with strong biological activity. The preformed values for the total inorganic carbon showed a good correlation with θ (r^2 = 0.962) and agreed with values obtained from other authors in the eastern Atlantic (Table 1). Our $NC_{T,bio}$ value for the AA of 2092 μmol kg^{-1} confirmed that the northward advection of AA is strongly diluted (<5% of pure AAIW) by MW and pENACW. MW was more ventilated during our cruise, as suggested by the AOU values compared with other values to the north of the Canary Islands with similar $C_{T,bio}$. The upwelling system can also favour the injection of nutrients, AOU and C_T to the water masses that advected southward. The 5% higher silicate values for lNADW compared with data obtained north of the Canary Islands may be the result of a deep silica maximum along 24ºN.

ACKNOWLEDGEMENTS

The authors thank all the participants in the Poseidon 257 cruise, and in particular the officers and crew of the research vessel. Special thanks are also due to the Laboratoire d'Etudes en Gèophysique et Océanographie Spatiale (LEGOS, Tolouse) for providing us with climatological wind and SST data at the ESTOC site and the SeaS Canarias-Departamento de Biología ULPGC-Viceconsejería de Pesca (GAC) for providing us with the SeaWIFS image in Figure 1. We would also like to thank Dr. F. Machín, who helped us with the development of the mixing model program. The article was much improved by the comments of two anonymous reviewers. This work was partially funded by the CARBOOCEAN 2005-2009, CN 511176-GOCE project and the MOMAC project (CTM2008-05914).

REFERENCES

Álvarez, M., F.F. Pérez, D.R. Shoosmith and H. L. Bryden. – 2005. Unaccounted role of Mediterranean Water in the drawdown of anthropogenic carbon. *J. Geophy. Res.*, 110: 1-18, doi: 10.1029/2004JC002633.

Arístegui, J., P. Sangrá, S. Hernández-León, M. Cantón, A. Hernández-Guerra and J.L. Kerling. – 1994. Island-Induced eddies in the Canary Islands. *Deep-Sea Res.*, 41: 1509-1525.

Arístegui, J., P. Tett, A. Hernández-Guerra, G. Basterretxea, M.F. Montero, K. Wild, P. Sangrá, S. Hernández-León, M. Cantón, J.A. García-Braun, M. Pacheco and E.D. Barton. – 1997. The influence of island-generated eddies on chlorophyll distribution: a study of mesoscale variation around Gran Canaria. *Deep-Sea Res*. I, 44: 71-96.

Arístegui, J., E.D. Barton, P. Tett, F.M. Montero, M. Garcia-Muñóz, G. Basterretxea, A. Cussatlegras, A. Ojeda and D. de Armas. – 2004. Variability in plankton community structure, metabolism, and vertical carbon fluxes along an upwelling filament (Cape Juby, NW Africa). *Prog. Oceanogr.,* 62 (2-4): 95-113.

Barton, E.D., J. Arístegui, P Tett, M. Cantón, J.G. Braun, S. Hernández-León, L. Nykjaer, C. Almeida, J. Almunia, S. Ballesteros, G. Basterretxea, J. Escánez, L. García-Weill, A. Hernández-Guerra, F. López-Laatzen, R. Molina, M.F. Montero, E. Navarro-Pérez, J.M. Rodríguez, K. van Lenning, H. Vélez and K. Wild. – 1998. The transition zone of the Canary Current upwelling region. *Prog. Oceanogr.*, 41: 455-504.

Barton, E.D., G. Basterretxea, P. Flament, E.G. Mitchelson-Jacob, B. Jones, J. Arístegui. and F. Herrera. – 2000. Lee region of Gran Canaria. *J. Geophys. Res.*, 105: 17173-17193.

Barton, E.D. and J. Arístegui. – 2004. The Canary Islands coastal transition zone-upwelling, eddies and filaments. *Prog. Oceanogr.,* 62(2-4): 67-69.

Basterretxea, G., E.D. Barton, P. Pett, P. Sangrá, E. Navarro-Pérez and J. Arístegui. – 2002. Eddy and deep chlorophyll maximum response to wind-shear in the lee of Gran Canaria. *Deep-Sea Res.,* 49: 1087-1101.

Boutin, J. and J. Echeto. – 1995. Estimating the chemical enhancement effect on the air-sea CO_2 exchange using the ERS1 scatterometer wind speeds, in Air-Water Gas Transfer. In: B.J.A.E.C. Monahan (ed.), pp. 827-841, AEON Verlag & Studio, Hanau, Germany.

Castro, C.G., F.F. Pérez, S.E. Holley and A.F. Ríos. – 1998. Chemical characterisation and modelling of water masses in the northeast Atlantic. *Prog. Oceanogr.*, 41: 249-279.

Chen, C.T.A., L.Y. Hsing, C.L. Liu and S.L. Wang. – 2004. Degree of nutrient consumption of upwelled water in the Taiwan Strait based on dissolved phosphorous or nitrogen. *Mar. Chem.,* 87: 73-86.

Clayton, T.D. and R.H. Byrne. – 1993. Spectrophotometric seawater pH measurements: Total hydrogen ion concentration scale calibration of m-cresol purple and at-sea results. *Deep-Sea Res.*, 40: 2115-2129.

Davenport, R., S. Neuer, A. Hernández-Guerra, M.J. Rueda, O. Llinás, G. Fisher and G. Wefer. – 1999. Seasonal and interannual pigment concentration in the Canary Islands region from CZCS data and comparison with observations from the ESTOC time-series station. *Int. J. Remote Sens.,* 20: 1419-1433.

Dickson, A.G. and F.J. Millero. – 1987. A comparison of the equilibrium-constants for the dissociation of carbonic-acid in seawater media. *Deep-Sea Res.*, 34 (10): 1733-1743.

DOE, 1994. In: A.G. Dickson and C. Goyet (eds.), *Handbook of Methods for the Analysis of the Various Parameters of the Carbon-Dioxide System in Sea Water*, 180 pp., ORNL/CDIAC-74.

Falkowski, P.G., D. Ziemann, Z. Kolber and P.K. Bienfang. – 1991. Role of eddy pumping in enhancing primary production in the ocean. *Nature*, 282: 677-680.

Fraga, F., E.D. Barton and O. Llinás. – 1985. The concentration of nutrient salts in "pure" North and South Atlantic Central Waters, In: Simposio Internacional Sobre las Area de Afloramiento más Importantes del Oeste Africano, Vol. 1, pp. 25-36, Instituto de Investigaciones Pesqueras, Barcelona, Spain.

Fraga, F., A.F. Ríos, F.F. Pérez and F.G. Figueiras. – 1998. Theoretical limits of oxygen:carbon and oxygen:nitrogen ratios during photosynthesis and mineralisation of organic matter in the sea. *Sci. Mar.*, 62(1-2): 161-168.

González-Dávila, M., J.M. Santana-Casiano, M. Rueda and O. Llinás. – 2003. Seasonal and interannual variability of sea surface carbon dioxide species at the European Station for Time Series in the Ocean at the Canary Islands (ESTOC) between 1996 and 2000, *Global Biogeochem. Cycles*, 17 (3): 1076.

González-Dávila, M., J.M. Santana-Casiano, D. de Armas and M. Suarez-Tangil. – 2006. The influence of island generated eddies on the carbon dioxide system, south of the Canary Islands. *Mar. Chem.*, 99: 177-190.

González-Dávila, M., Santana-Casiano, J.M. and E.F. González-Dávila. – 2007. Interannual variability of the upper ocean carbon cycle in the northeast Atlantic Ocean. *Geophys. Res. Lett.*, 34(7): L07608.

Hammersley, J.M. and D.C. Handscomb. – 1964. *Monte Carlo Methods*. John Wiley & Sons, New York, 177 pp.

Hansen, H.P. and K. Grasshoff. – 1983. Automated chemical analysis. In: *Methods of Seawater Analysis*, pp. 368-376. Verlag Chemie, Weinheim.

Harvey, J. – 1982. θ-S relationship and water masses in the eastern North Atlantic. *Deep-Sea Res.,* 29(8A): 1021-1033.

Käse, R. H., J.F. Prince, P.L. Richardson and W. Zenk. – 1986. A quasi-synoptic survey on the thermocline circulation and water masses distribution within the Canary Basin. *J. Geophys. Res.*, 91: 9739-9748.

Le Groupe CITHER-3. – 1998. Recueil de données. Volume 3: Traceurs Géochimiques. 586 pp. Rapport Interne LPO (98-03)

Lee, K., R. Wanninkhof and R. Feely. – 1998. Carbon Dioxide, Hydrographic, and Chemical Data Obtained During the R/V Ronald Brown in the Atlantic Ocean During WOCE Line AR01 (A05) (23 Jan. - 24 Feb., 1998).

Longhurst, A. – 1998. *Ecological Geography of the Sea*. Academic Press, San Diego and London.

Machín, F. and J.L. Pelegrí. – 2009. Northward penetration of Antarctic intermediate water off northwest Africa. *J. Phys. Oceanogr.*, 39: 512-535.

McCartney, M. and T. Talley. – 1982. The subpolar mode water of the North Atlantic Ocean. *J. Phys. Oceanogr.*, 12: 1169-1188.

McGillicuddy, Jr., D.J., Anderson, L.A., Doney, S.C. and M.E. Maltrud. – 2003. Eddy-driven sources and sinks of nutrients in the upper ocean: results from 0.1 degree resolution model of the North Atlantic. *Global Biogeochem. Cycles,* 17(2): 1035, doi:10.1029/2002GB001987.

Mehrbach, C., C.H. Culberso, J.E. Hawley and R.M. Pytkowic. – 1973. Measurements of apparent dissociation-constants of carbonic-acid in seawater at atmospheric-pressure. *Limnol. Oceanogr.*, 18(6): 897-907.

Mintrop, L., F.F. Perez, M. Gonzalez-Davila, J.M. Santana-Casiano and A. Körtzinger. – 2000. Alkalinity determination by potentiometry: Intercalibration using three different methods. *Cienc. Mar.,* 26(1): 23-37.

Paillet, J., M. Arhan and M.S. McCartney. – 1998. Spreading of Labrador Sea Water in the eastern North Atlantic. *J. Geophys. Res.*, 103(C5): 10223-10239.

Pérez, F.F., A.F. Ríos, C.G. Castro and F. Fraga. – 1998. Mixing analysis of nutrients, oxygen and dissolved inorganic carbon in the upper and middle North Atlantic ocean east of the Azores. *J. Mar. Syst.*, 16(3-4): 219-233.

Pérez, F.F., L. Mintrop, O. Linás, M. González-Dávila, C.G. Castro, M. Álvarez, A. Körtzinger, J.M. Santana-Casiano, M.J. Rueda and A.F. Ríos. – 2001. Mixing analysis of nutrients, oxygen and inorganic carbon in the Canary Islands region. *J. Mar. Syst.*, 28: 183-201.

Pollard, R.T., M.J. Griffiths, S. Cunningham, J.F. Read, F.F. Pérez and A.F. Ríos. – 1996. Vivaldi 1991 - A study of the formation, circulation and ventilation of Eastern North Atlantic Central Water. *Prog. Oceanogr.*, 37: 167-192.

Reid, J.L. – 1994. On the total geostrophic circulation of the North Atlantic Ocean: Flow patterns, tracers and transports. *Prog. Oceanogr.,* 33: 1-92.

Reynolds, R.W. and T.M. Smith. – 1994. Improved global sea surface temperature analyses using optimum interpolation. *J. Clim.,* 7: 929-948.

Ríos, A.F., F.F. Pérez and F. Fraga. – 1992. Water masses in the upper and middle North Atlantic Ocean east of the Azores. *Deep-Sea Res.* Part A, 39: 645-658.

Ríos, A.F., F. Fraga, F.G. Figueiras and F.F. Pérez. – 1998. A modeling approach to the Redfield ratio deviations in the ocean. *Sci. Mar.,* 62(1-2):169-176.

Santana-Casiano J.M., M. González-Dávila, L.M. Laglera-Baquer and M.J. Rodríguez-Somoza. – 2001. Carbon dioxide system in the Canary region during October 1995. *Sci. Mar.,* 65: 41-49.

Santana-Casiano J.M., M. González-Dávila, M.J. Rueda, O. Llinás and E. González-Dávila. – 2007. The interannual variability of the oceanic CO_2 parameters in the northeast Atlantic subtropical gyre at the ESTOC site. *Global Biogeochem. Cycles*, 21(1), Art. Nº GB1015.

Siedler, G., A. Kuhl and W. Zenk. – 1987. The Madeira Mode Water. *J. Phys. Oceanogr.*, 17: 1561-1970.

Speer, K.G. – 1993. The deep silica tongue in the North Atlantic. *Deep-Sea Res.,* 40: 925-936.

Takahashi, T., J. Olafsson, J.G. Goddard, D.W. Chipman and S.C. Sutherland. – 1993. Seasonal variation of CO_2 and nutrient in the high latitude surface oceans: a comparative study. *Global Biogeochem. Cycles*, 7: 843-878.

Tomczak, M. – 1981. An analysis of mixing in the frontal zone of South and North Atlantic central water off northwest Africa. *Prog. Oceanogr.*. 10: 172-192.

Touratier, F., L. Azouzi and C. Goyet. – 2007. CFC-11, $\Delta^{14}C$ and ^{3}H tracers as a means to assess anthropogenic CO_2 concentrations in the ocean. *Tellus B,* 59: 318-325.

Tsuchiya, M., L.D. Talley and M.S. McCartney. – 1992. An eastern Atlantic section from Iceland southward across the equator. *Deep-Sea Res.*, 39: 1885-1917.

Wanninkhof, R. – 1992. Relationship between wind-speed and gas-exchange over the Ocean. *J. Geophys. Res.,* 97 (C5), 7373-7382.

Wanninkhof, R. and K. Thoning. – 1993. Measurement of fugacity of CO_2 in surface-water using continuous and discrete sampling methods. *Mar. Chem.*, 44(2-4): 189-204.

Welschmeyer, N.A. – 1994. Fluorometric analysis of chlorophyll *a* in presence of chlorophyll *b* and phaeopigments. *Limnol. Oceanogr.*, 39: 1985-1992.

WOCE. 1994. *WOCE Operations Manual, Section 3.1*. WOCE Hydrographic Programme, World Ocean Circulation Experiment.

Wright, R.W. and L.V. Worthington. – 1970. *The water masses of the North Atlantic Ocean: a volumetric census of temperature and salinity.* American Geophysical Society, Series Atlas of the Marine Environment, Vol. 19.

Wüst, G. and A. Defant. – 1936. Atlas of the stratification and circulation of the Atlantic Ocean. *Sci. Res. German Atlantic exp. R.V. Meteor, 1925-1927*, Vol. 6.

Received November 1, 2008. Accepted July 30, 2010.
Published online November 13, 2010.